Highly Conductive, Mechanically Robust, and Electrochemically Inactive TiC/C Nanofiber Scaffold for High-Performance Silicon Anode Batteries

Yan Yao,[†,∥] Kaifu Huo,[†,∥] Liangbing Hu,[†] Nian Liu,[‡] Judy J. Cha,[†] Matthew T. McDowell,[†] Paul K. Chu,[§] and Yi Cui[†,⊥,*]

[†]Department of Materials Science and Engineering, Stanford University, Stanford, California 94305, United States, [‡]Department of Chemistry, Stanford University, Stanford, California 94305, United States, [§]Department of Physics and Materials Science, City University of Hong Kong, Hong Kong, China, and [⊥]Stanford Institute for Materials and Energy Sciences, SLAC National Accelerator Laboratory, 2575 Sand Hill Road, Menlo Park, California 94025, United States. [∥]These authors contributed equally to this work.

ABSTRACT Silicon has a high specific capacity of 4200 mAh/g as lithium-ion battery anodes, but its rapid capacity fading due to >300% volume expansion and pulverization presents a significant challenge for practical applications. Here we report a core–shell TiC/C/Si inactive/active nanocomposite for Si anodes demonstrating high specific capacity and excellent electrochemical cycling. The amorphous silicon layer serves as the active material to store Li^+, while the inactive TiC/C nanofibers act as a conductive and mechanically robust scaffold for electron transport during the Li–Si alloying process. The core–shell TiC/C/Si nanocomposite anode shows ~3000 mAh g^{-1} discharge capacity and 92% capacity retention after 100 charge/discharge cycles. The excellent cycling stability and high rate performance could be attributed to the tapering of the nanofibers and the open structure that allows facile Li ion transport and the high conductivity and mechanical stability of the TiC/C scaffold.

KEYWORDS: titanium carbide · conductive scaffold · silicon anode · lithium-ion batteries · cycling stability

Developing Li-ion batteries with higher storage capacity, faster charging rate, greater cycling stability, and higher power is essential for next-generation electrical vehicles.[1−10] Silicon is considered one of the most promising anode materials due to its high theoretical specific capacity (4200 mAh g^{-1}, 10 times that of commercial graphite anodes), high volumetric capacity (9786 mAh cm^{-3}), low cost, and environmental safety.[11−19] However, conventional Si anodes typically suffer from poor capacity retention due to mechanical fracture caused by large volume expansion during the alloying reaction of Si ($Si + xLi^+ + xe^- \leftrightarrow Li_xSi$ ($0 \le x \le 4.4$)), limiting their cycle life and application in high-power devices such as electric vehicles.[20,21]

In recent years, nanostructured materials, such as homogeneous Si nanowires[12,13] and hybrid Si core–shell nanowires,[22,23] have been utilized to obtain good cycling performance. Our group used crystalline Si nanowires (NWs) grown directly on a metal current collector as an anode, resulting in high specific capacity and cycling stability because the small diameter of NWs allows for better accommodation of the large volume changes without fracture.[12] In addition, each Si NW is electrically connected to the metallic current collector so that all the NWs contribute to the capacity. Following this study, active/inactive core/shell Si-based nanostructured anodes were found to further improve cycle life and power rate, such as crystalline–amorphous Si NWs,[22] $TiSi_2$/Si nanonets,[23] and carbon/Si NWs.[24] However, these anodes still have some disadvantages and could be improved. For the crystalline–amorphous Si NW anodes[22] and $TiSi_2$/Si nanonets,[23] the core materials are not truly inert. Crystalline Si could react with Li at a lower potential (120 mV) than that of a-Si (230 mV),[22] and $TiSi_2$ reacts with Li at 60–70 mV.[23] Therefore, these structures can cycle well only when the charging potential is limited to selectively lithiate the shell; otherwise their capacity will fade with cycles due to lithiation of the core material. Thus, a portion of the full capacity of Si may be wasted; in addition, strict voltage control for selective lithiation of the shell material is not quite feasible in practical batteries.

Here we demonstrate a new anode based on a TiC/C/Si core/shell structure in which the highly conductive and robust core–shell TiC/C nanowire arrays are rooted onto

* Address correspondence to yicui@stanford.edu.

Received for review September 1, 2011 and accepted October 5, 2011.

Published online October 05, 2011
10.1021/nn2033693

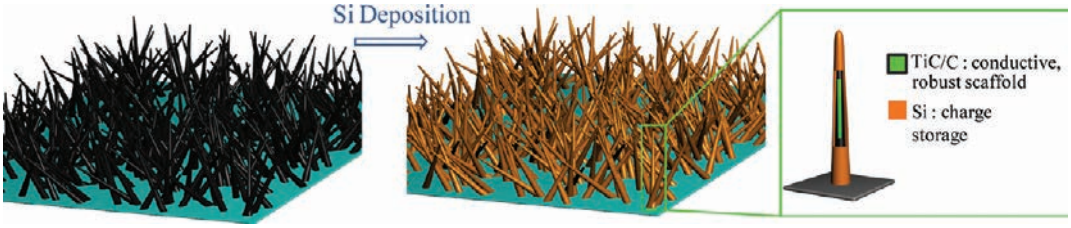

Figure 1. Schematic illustrating the fabrication process of a TiC/C nanofiber scaffold for Si anode architecture. TiC/C nanofibers (green/black) provide a conductive, mechanically robust scaffold, and the Si coating (orange) functions as a charge-storage layer.

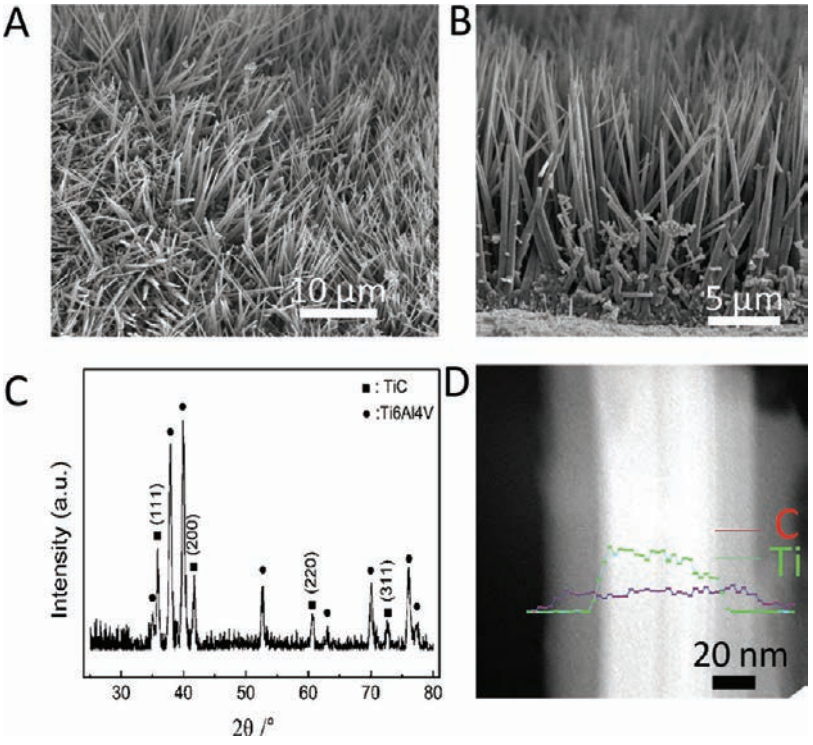

Figure 2. (A) Typical tilted SEM image of TiC/C nanofibers. (B) Cross-sectional SEM image of TiC/C nanofibers showing all nanofibers are rooted to the substrate. (C) XRD of TiC/C nanofibers with peaks from the Ti6Al4 V substrate. (D) Dark field STEM image of a single TiC/C nanofiber with an EDX line scan profile of C (red) and Ti (green).

the metal current collector as the inert scaffold, and the outer Si shell serves as the active material to store Li^+. This inactive/active nanocomposite design decouples lithium storage and charge transport, thus resulting in excellent cycling stability and high rate performance. In half-cells, these electrodes have 92% capacity retention after 100 charge/discharge cycles and show ~3000 mAh g^{-1} specific discharge capacity (in Si mass). The fact that individual TiC/C NW remains vertically rigid after tens of charge/discharge cycles is attributed to its highly robust mechanical properties; this persistent mechanical integrity has not been observed in other nanostructured Si anodes.

The core/shell nanocomposite electrode design is shown in Figure 1. The TiC/C nanofiber scaffold was produced by a simple thermochemical process, and it provides mechanical support as well as superior charge transport for the active amorphous Si layer. The amorphous Si functions as the Li storage layer and is uniformly coated on the scaffold surface by chemical vapor deposition (CVD). TiC is an extremely hard material (Mohs hardness 9−9.5) with very low resistivity (6.8×10^{-5} Ω·cm).[25] In addition, TiC/C does not react with lithium,[26] which is confirmed by our cyclic voltammetry (CV) measurements (Figure 4A). A thin film of a-Si can be uniformly coated on the high surface area of the TiC/C nanofibers scaffold, and the weight ratio of the Si layer to the scaffold can be controlled by adjusting the a-Si thickness. In this way, the thickness of the Si layer can be less than the fracture threshold so as to preserve its structural integrity during battery cycling. This paper provides a new route to design novel high-performance nanostructured electrodes for Li-ion batteries by combining a highly robust, inert, and conductive nanocomposite scaffold with an active layer to store Li-ions.

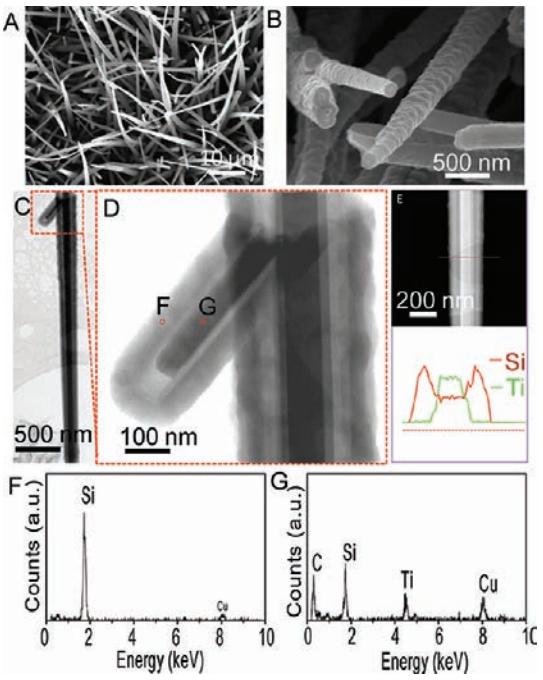

Figure 3. (A) Typical tilted SEM image of TiC/C/Si nanocomposite electrodes. (B) Magnified SEM image showing the tip of the nanofibers. (C) Bright field STEM image of a single TiC/C/Si nanocomposite. (D) Magnified bright field STEM image, revealing the trilayer structure with contrast due to atomic number. (E) Dark field STEM image and the EDX line scan profile of Si (red) and Ti (green). (F, G) EDX spectroscopy at two spots located in the Si shell (F) and TiC core (G), respectively. Cu signal is from the Cu TEM grid.

RESULTS AND DISCUSSION

The core–shell TiC/C nanofiber arrays were grown directly on a Ti alloy (Ti6Al4 V) foil under acetone vapor at 850 °C by thermochemical reaction in one step.[27] A thin layer of a-Si was further deposited by CVD to form TiC/C/Si nanofibers, as schematically shown in Figure 1. Typical scanning electron microscopy (SEM) images of an as-fabricated nanofiber scaffold (Figure 2A and B) suggest that the tapered nanofibers, which are 10–15 μm in length and 80–180 nm in diameter tapering from the base to tip, are rooted onto the substrate with a quasi-aligned morphology. An X-ray diffraction pattern of a TiC/C scaffold is displayed in Figure 2C. The diffraction peaks can be indexed to the cubic TiC structure besides the peaks from the substrate.[27] The dark field scanning transmission electron microscopy (STEM) image reveals that the nanofiber has a core–shell structure (Figure 2D), which is also confirmed by the energy dispersive X-ray spectroscopy (EDX) line scan profile of C and Ti in the inset of Figure 2D. The TiC core appears brighter since the intensity in STEM scales with the atomic number (Ti has the highest atomic number in this structure) and the shell is carbon. The radius of the TiC core is ~30 nm, and the carbon shell thickness is ~20–40 nm.

Figure 3A shows the morphology of the TiC/C/Si nanocomposite electrode after 20 min of a-Si deposition. The conical TiC/C scaffold provides enough open space for conformal coating of Si from the bottom to the top. This could be difficult to realize in some vertically arranged CNT arrays because the spacing between CNTs is too narrow to allow uniform Si coating on individual CNTs.[28] A high-magnification SEM image in Figure 3B shows that the Si has a moderately rough surface and that the Si coating layer at the end of the fiber tips is ~60 nm thick. The three-layer structure of a single composite nanofiber is easily visible in bright field STEM images (Figure 3C and D). Since the contrast is related to the atomic number difference, the TiC core appears darker, as it is heavier than carbon and Si. The Si shell thickness is ~60 nm, similar to that observed in the SEM. The EDX spectra from the shell (Figure 3F) and from the core (Figure 3G) indicate that the shell is Si and the inner core is TiC. The existence of Si in the latter spectrum is due to an electron beam passing through the top and bottom shell. This is further confirmed by the intensity profile of Si and Ti in the EDX line scan profile (Figure 3E).

After fabrication, we evaluated the electrochemical Li storage capability of the TiC/C/Si nanocomposite. Figure 4A shows typical CV curves of the TiC/C scaffold before and after Si deposition over the potential window of 0.01–1 V at a scan rate of 0.1 mV s^{-1}. Before Si deposition, the curve shows double layer capacitor behavior and no peak related to lithiation of TiC/C is observed, which confirms the inactive nature of the scaffold.[26] After Si deposition, the CV curve changes shape dramatically and peaks related to (de)lithiation of Si are observed. The peak at 0.19 V in the cathodic branch is due to the conversion of a-Si to an amorphous Li_xSi phase.[29] The two peaks at 0.41 and 0.55 V in the anodic branch correspond to delithiation of a-Li_xSi to a-Si.[29]

Coin-type half-cells were fabricated using lithium foil as the counter electrode and the TiC/C/Si nanocomposite grown on the Ti alloy collector as the working electrode. Celgard 2250 polymer separators were employed. No binders or carbon black conductive additives were used. As the electrolyte, 1.0 M $LiPF_6$ in 1:1 w/w ethylene carbonate/diethyl carbonate (Novolyte Technologies) was used. Figure 4B shows the voltage profiles for the first, second, and 100th galvanostatic charge/discharge cycles. For the first cycle at a rate of C/5 (0.84 A/g), the charge and discharge capacity reaches 4180 and 3066 mAh g^{-1} (in Si mass), and the Coulombic efficiency (CE) is 72%. The irreversible capacity ratio of 28% may be attributed to the formation of a solid electrolyte inter-phase (SEI) on the electrode surface as suggested by a short plateau at 0.4 V with ~1000 mAh/g capacity shown in Figure 4B. The formation of the SEI layer would consume Li^+, which contributes to the irreversible capacity during the first cycle. The SiO_x layer formed on the Si surface during the exposure to air is another reason resulting in

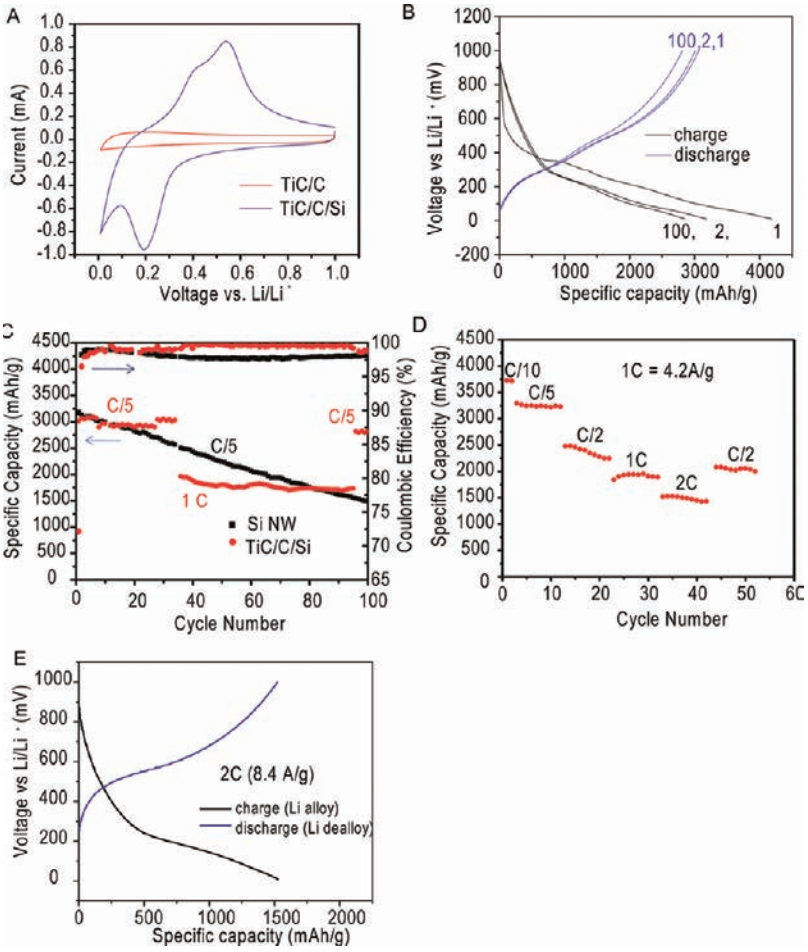

Figure 4. Electrochemical performance of a TiC/C/Si nanocomposite electrode. (A) Typical cyclic voltammetry curve comparison of the TiC/C scaffold before and after Si deposition, showing the inert nature of TiC with Li^+. (B) Galvanostatic charge−discharge voltage profile between 0.01 and 1 V *vs* Li/Li^+ for the first, second, and 100th cycle at C/5 (0.84 A/g) rate. (C) Discharge specific capacity *vs* cycle number for 100 cycles at a rate of C/5 and 1C (4.2 A/g) in comparison with Si NWs. Only the mass of Si is considered for specific capacity calculation. (D) Discharge specific capacity *vs* cycle number at C/10, C/5, C/2, 1C, and 2C rates (1C = 4.2 A/g) with voltage cutoffs of 0.01 and 1 V. The same rates are used for both discharge and charge. (E) Galvanostatic charge−discharge voltage profile for a typical cycle at 2C (8.4 A/g) rate. All measurements were carried out at room temperature in two-electrode 2032 coin-type half-cells.

the irreversible capacity. The discharge capacity for the second and the 100th cycles is 3048 and 2812 mAh g^{-1}, respectively, corresponding to 2% and 8% decay from the first cycle. The fact that the capacity degrades only 0.08% per cycle indicates the superior stability of the electrode. Figure 4C shows the cycling performance of the same TiC/C/Si electrode coin cell for 100 cycles. After 35 cycles at a rate of C/5, the discharge capacity remains around 3000 mAh g^{-1} and the CE is 99.0%. Increasing the current to 1C for 60 cycles causes the capacity to decrease to 1730 mAh g^{-1}, while the CE increases to 99.6%. Further cycling at C/5 brings the capacity back to a reversible value of 2800 mAh g^{-1}, which results in 92% capacity retention over 100 cycles. When the total mass is considered, the TiC/C/Si anode shows the discharge capacity of 1800 mAh/g for the first cycle, and it remains 1680 mAh/g after 100 cycles. In comparison, the Si NW anode shows 3100 mAh/g for the first cycle and degrades to 1400 mAh g^{-1} over the same number of cycles (Figure 4C). Similar degradation for Si NWs was also reported in ref 30, showing ~1500 mAh/g capacity remaining after 80 cycles. Hence, the TiC/C/Si anode shows better capacity and stability over a Si NW anode even when total mass is considered. The discharge capacity behavior reported here was reproducible over many coin cells. Another example of the electrochemical behavior of the TiC/C/Si electrode is shown in Figure 4D, where the cell is cycled continuously at various C rates (C/10, C/5, C/2, 1C, and 2C, where 1C = 4.2 A/g). The discharge capacities at each rate are 3710, 3240, 2360, 1910, and 1500 mAh g^{-1}, respectively. The discharge capacities at 1C and 2C were 59% and 46% of the C/5 capacity, respectively. The voltage profile at 2C rate (8.4 A/g) is shown in Figure 4E. A typical sloping feature in the charge/discharge curve of a-Si is clearly distinguishable at this rate, indicating lithiation (delithiation) of a-Si to an amorphous Li_xSi. The retaining capacity of 1500 mAh

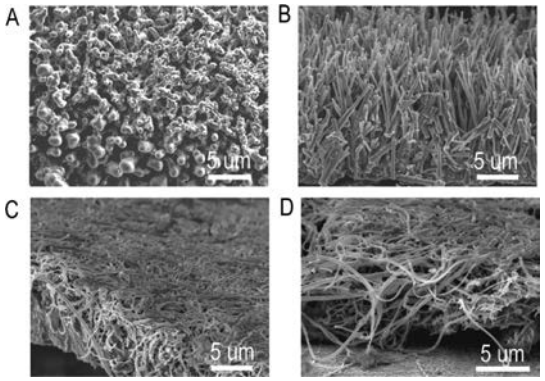

Figure 5. (A) SEM image of TiC/C/Si electrode after 50 charge/discharge cycles and rinsing in acetonitrile to remove residue electrolyte. (B) SEM image after second rinsing in 1 M HCl to remove SEI. (C) SEM image of Si NWs after 50 charge/discharge cycles and rinsing in acetonitrile to remove residue electrolyte. (D) SEM image after second rinsing in 1 M HCl to remove SEI.

g^{-1} at 2C is four times that of the theoretical capacity of graphite. The high rate capacity can be attributed to the high conductivity and mechanical properties of the TiC/C nanofiber scaffold used in the electrode.

The excellent cycling stability and high rate performance of this electrode are possibly due to (1) the tapering of the nanofibers and the open structure between the fibers that allows for facile Li^+ transport and (2) the highly conductive and mechanical stability of TiC so that the anode could remain in the aligned morphology during the cycling. These effects were studied in the following manner. First, cells were opened in a glovebox after 50 charge/discharge cycles, and the morphology of the anodes was studied with SEM. Figure 5A,B show the morphology before and after removing the solid electrolyte interphase by rinsing in 1 M HCl. The durability of the nanofibers is clear: all the nanofibers were still standing straight after 50 cycles. Since there is no reaction between TiC and Li^+, the core of the nanofibers remains rigid after cycling. The excellent physical and electrical contact of nanofibers with the substrate and good electrochemical stability enable this cycling stability and fast charge transport. This is in contrast to the case of Si NWs, where most nanowires are pressed down onto the substrate, as shown in Figure 5C and D. Lithium insertion into Si breaks Si–Si bonds and forms weaker Li–Si bonds, resulting in a decrease in Young's modulus, a reduction in yield strength, and a brittle-to-ductile transition.[31] This deterioration in mechanical properties, along with the volume changes that occur during lithiation, can cause pure NWs to warp and become a dense mass of wires packed between the separator and current collector with cycling, which can cause a decline in capacity, especially if some Si becomes electrically isolated.[32]

CONCLUSIONS

In summary, a novel TiC/C/Si nanocomposite nanofiber anode was fabricated, and it demonstrated excellent cycling stability and high specific capacity. A stable discharge capacity of ~2800 mAh g^{-1} was retained after 100 cycles of charge/discharge. The capacity degrades only 0.08% per cycle over 100 cycles. The mechanical integrity of the TiC/C scaffold was shown even after 50 charge/discharge cycles. This active/inactive nanocomposite design decouples lithium storage and charge transport, thus leading to improved cycling stability and rate performance.

MATERIALS AND METHODS

Synthesis of TiC/C/Si Nanocomposite Structures. Ti6Al4 V foils (10 × 10 × 1 mm^3, Advent, 99.5%) were degreased ultrasonically in acetone and ethanol sequentially. After rinsing with double-distilled water and drying under flowing nitrogen, the Ti6Al4 V foil was loaded onto a ceramic boat placed in the center of a quartz tube in a horizontal tube furnace. The reactor was purged with pure argon several times to remove residual oxygen and moisture before heating to 850 °C under Ar. Acetone was then introduced into the chamber by bubbling with argon at a flow rate of 150 sccm. After 1.5 h, the tube was cooled to room temperature under flowing argon, and the sample of core–shell TiC/C nanofiber arrays is formed on the Ti alloy substrate. To form the outer Si shell, the TiC/C nanofibers on substrates were transferred into a quartz tube furnace (1 in. diameter) for low-pressure chemical vapor deposition of a-Si. The sample was heated to 495 °C, and silane (SiH_4, 2% in argon) was flowed in at 50 sccm with a total chamber pressure of 30 Torr for 40 min. The mass of a-Si was calculated by measuring the substrate on a microbalance (Sartarious SE2, 0.1 μg resolution) before and after the synthesis. The final silicon mass loading is ~0.4 mg/cm^2, which is ~60% of the total mass including the TiC/C scaffold.

Electrochemical and Structural Characterization. The as-formed TiC/C/Si nanocomposite electrodes were quickly transferred to an argon-filled glovebox for cell making. Standard coin cells (2033) were made using a lithium foil as the counter electrode and Celgard 2250 as the separator. No binders or carbon black was used. As the electrolyte, 1.0 M $LiPF_6$ in 1:1 w/w ethylene carbonate/diethyl carbonate (Novolyte Technologies) was used. All measurements were made using a Biologic VMP3 battery tester. Galvanostatic cycling was performed with voltage cutoffs of 1.0 and 0.01 V *vs* Li/Li^+, and cyclic voltammetry was performed between 1.0 and 0.01 V *vs* Li/Li^+ at a rate of 0.05 mV s^{-1}. Scanning electron microscopy (SEM, FEI XL30 Sirion), transmission electron microscopy (TEM, 200 kV FEI Tecnai F20), and X-ray diffraction (XRD, PANalaytical X'Pert) were used to characterize the material.

Acknowledgment. This work was partially supported by the Assistant Secretary for Energy Efficiency and Renewable Energy, Office of Vehicle Technologies of the U.S. Department of Energy, under Contract No. DE-AC02-05CH11231, Subcontract No. 6951379 under the Batteries for Advanced Transportation Technologies (BATT) Program. A portion of this work is also supported by the Department of Energy, Office of Basic Energy Sciences, Division of Materials Sciences and Engineering, under Contract DE-AC02-76SF0051, through the SLAC National Accelerator Laboratory LDRD project. Y.C. acknowledges support from the King Abdullah University of Science and Technology Investigator Award (No. KUS-I1-001-12). K.H. acknowledges support from National Natural Science Foundation of China (No. 50902104), City University of Hong Kong Strategic

Research Grant No. 7008009, and China Scholarship Council (No. 2010842443).

REFERENCES AND NOTES

1. Rolison, D. R.; Nazar, L. F. Electrochemical Energy Storage to Power the 21st Century. *MRS Bull.* **2011**, *36*, 486–493.
2. Goodenough, J. B.; Kim, Y. Challenges for Rechargeable Li Batteries. *Chem. Mater.* **2010**, *22*, 587–603.
3. Bruce, P. G.; Scrosati, B.; Tarascon, J. M. Nanomaterials for Rechargeable Lithium Batteries. *Angew. Chem., Int. Ed.* **2008**, *47*, 2930–2946.
4. Liu, J.; Cao, G.; Yang, Z.; Wang, D.; Dubois, D.; Zhou, X.; Graff, G. L.; Pederson, L. R.; Zhang, J.-G. Oriented Nanostructures for Energy Conversion and Storage. *ChemSusChem* **2008**, *1*, 676–697.
5. Oumellal, Y.; Rougier, A.; Nazri, G. A.; Tarascon, J. M.; Aymard, L. Metal Hydrides for Lithium-Ion Batteries. *Nat. Mater.* **2008**, *7*, 916–921.
6. Sun, Y. K.; Myung, S. T.; Park, B. C.; Prakash, J.; Belharouak, I.; Amine, K. High-Energy Cathode Material for Long-life and Safe Lithium Batteries. *Nat. Mater.* **2009**, *8*, 320–324.
7. Huang, J. Y.; Zhong, L.; Wang, C. M.; Sullivan, J. P.; Xu, W.; Zhang, L. Q.; Mao, S. X.; Hudak, N. S.; Liu, X. H.; Subramanian, A.; *et al*. In Situ Observation of the Electrochemical Lithiation of a Single SnO_2 Nanowire Electrode. *Science* **2010**, *330*, 1515–1520.
8. Ji, X.; Evers, S.; Black, R.; Nazar, L. F. Stabilizing Lithium-Sulphur Cathodes Using Polysulphide Reservoirs. *Nat. Commun.* **2011**, *2*, 325.
9. Zhang, H.; Yu, X.; Braun, P. V. Three-Dimensional Bicontinuous Ultrafast-Charge and Discharge Bulk Battery Electrodes. *Nat. Nanotechnol.* **2011**, *6*, 277–281.
10. Malik, R.; Zhou, F.; Ceder, G. Kinetics of Non-Equilibrium Lithium Incorporation in $LiFePO_4$. *Nat. Mater.* **2011**, *10*, 587–590.
11. Obrovac, M. N.; Krause, L. J. Reversible Cycling of Crystalline Silicon Powder. *J. Electrochem. Soc.* **2007**, *154*, A103–A108.
12. Chan, C. K.; Peng, H. L.; Liu, G.; McIlwrath, K.; Zhang, X. F.; Huggins, R. A.; Cui, Y. High-Performance Lithium Battery Anodes Using Silicon Nanowires. *Nat. Nanotechnol.* **2008**, *3*, 31–35.
13. Peng, K.; Jie, J.; Zhang, W.; Lee, S. T. Silicon Nanowires for Rechargeable Lithium-Ion Battery Anodes. *Appl. Phys. Lett.* **2008**, *93*, 033105.
14. Magasinski, A.; Dixon, P.; Hertzberg, B.; Kvit, A.; Ayala, J.; Yushin, G. High-Performance Lithium-Ion Anodes Using a Hierarchical Bottom-Up Approach. *Nat. Mater.* **2010**, *9*, 353–358.
15. Song, T.; Xia, J. L.; Lee, J. H.; Lee, D. H.; Kwon, M. S.; Choi, J. M.; Wu, J.; Doo, S. K.; Chang, H.; Il Park, W.; *et al.* Arrays of Sealed Silicon Nanotubes as Anodes for Lithium Ion Batteries. *Nano Lett.* **2010**, *10*, 1710–1716.
16. Kim, H.; Seo, M.; Park, M. H.; Cho, J. A Critical Size of Silicon Nano-Anodes for Lithium Rechargeable Batteries. *Angew. Chem., Int. Ed.* **2010**, *49*, 2146–2149.
17. Choi, N.-S.; Yao, Y.; Cui, Y.; Cho, J. One Dimensional Si/Sn-Based Nanowires and Nanotubes for Lithium-Ion Energy Storage Materials. *J. Mater. Chem.* **2011**, *21*, 9825–9840.
18. McDowell, M. T.; Cui, Y. Single Nanostructure Electrochemical Devices for Studying Electronic Properties and Structural Changes in Lithiated Si Nanowires. *Adv. Ener. Mater.* **2011**, *1*, 894–900.
19. Cui, L.-F.; Hu, L.; Choi, J. W.; Cui, Y. Light-Weight Free-Standing Carbon Nanotube-Silicon Films for Anodes of Lithium Ion Batteries. *ACS Nano* **2010**, *4*, 3671–3678.
20. Huggins, R. A. Lithium Alloy Negative Electrodes. *J. Power Sources* **1999**, *81*, 13–19.
21. Beaulieu, L. Y.; Eberman, K. W.; Turner, R. L.; Krause, L. J.; Dahn, J. R. Colossal Reversible Volume Changes in Lithium Alloys. *Electrochem. Solid State Lett.* **2001**, *4*, A137–A140.
22. Cui, L. F.; Ruffo, R.; Chan, C. K.; Peng, H. L.; Cui, Y. Crystalline-Amorphous Core-Shell Silicon Nanowires for High Capacity and High Current Battery Electrodes. *Nano Lett.* **2009**, *9*, 491–495.
23. Zhou, S.; Liu, X.; Wang, D. Si/$TiSi_2$ Heteronanostructures as High-Capacity Anode Material for Li Ion Batteries. *Nano Lett.* **2010**, *10*, 860–863.
24. Cui, L. F.; Yang, Y.; Hsu, C. M.; Cui, Y. Carbon-Silicon Core-Shell Nanowires as High Capacity Electrode for Lithium Ion Batteries. *Nano Lett.* **2009**, *9*, 3370–3374.
25. Leroy, W. P.; Detavernier, C.; Meirhaeghe, R. L. V.; Kellock, A. J.; Lavoie, C. Solid-State Formation of Titanium Carbide and Molybdenum Carbide as Contacts for Carbon-Containing Semiconductors. *J. Appl. Phys.* **2006**, *99*, 063704.
26. Park, C.-M.; Sohn, H.-J. Electrochemical Characteristics of $TiSb_2$ and Sb/TiC/C Nanocomposites as Anodes for Rechargeable Li-Ion Batteries. *J. Electrochem. Soc.* **2010**, *157*, A46–A49.
27. Hu, L.; Huo, K.; Chen, R.; Zhang, X.; Fu, J.; Chu, P. K. Core-Shell TiC/C Quasi-Aligned Nanofiber Arrays on Biomedical Ti6Al4V for Sensitive Electrochemical Biosensing. *Chem. Commun.* **2010**, *46*, 6828–6830.
28. Welna, D. T.; Qu, L.; Taylor, B. E.; Dai, L.; Durstock, M. F. Vertically Aligned Carbon Nanotube Electrodes for Lithium-Ion Batteries. *J. Power Sources* **2011**, *196*, 1455–1460.
29. Li, J.; Dahn, J. R. An In Situ X-ray Diffraction Study of the Reaction of Li with Crystalline Si. *J. Electrochem. Soc.* **2007**, *154*, A156–A161.
30. Chan, C. K.; Ruffo, R.; Hong, S. S.; Cui, Y. Surface Chemistry and Morphology of the Solid Electrolyte Interphase on Silicon Nanowire Lithium-Ion Battery Anodes. *J. Power Sources* **2009**, *189*, 1132–1140.
31. Shenoy, V. B.; Johari, P.; Qi, Y. Elastic Softening of Amorphous and Crystalline Li-Si Phases with Increasing Li Concentration: A First-Principles Study. *J. Power Sources* **2010**, *195*, 6825–6830.
32. Ruffo, R.; Hong, S. S.; Chan, C. K.; Huggins, R. A.; Cui, Y. Impedance Analysis of Silicon Nanowire Lithium Ion Battery Anodes. *J. Phys. Chem. C* **2009**, *113*, 11390–11398.
33. Balke, N.; Jesse, S.; Kim, Y.; Adamczyk, L.; Tselev, A.; Ivanov, I. N.; Dudney, N. J.; Kalinin, S. V. Real Space Mapping of Li-Ion Transport in Amorphous Si Anodes with Nanometer Resolution. *Nano Lett.* **2010**, *10*, 3420–3425.